



## **Lost in homogenisation: Navigating the challenges of predicting ideal behaviour in inhomogeneous porous structures**

Downloaded from: <https://research.chalmers.se>, 2025-07-01 15:24 UTC

Citation for the original published paper (version of record):

Wagner, M., Wurm, S., Baumann, G. et al (2025). Lost in homogenisation: Navigating the challenges of predicting ideal behaviour in inhomogeneous porous structures. *International Journal of Solids and Structures*, 320. <http://dx.doi.org/10.1016/j.ijsolstr.2025.113522>

N.B. When citing this work, cite the original published paper.



## Lost in homogenisation: Navigating the challenges of predicting ideal behaviour in inhomogeneous porous structures

Markus Wagner<sup>a</sup>, Sebastian Wurm<sup>a</sup>, Georg Baumann<sup>a</sup>, Tiina Nypelö<sup>b,c</sup>, Florian Feist<sup>a,\*</sup>

<sup>a</sup> Vehicle Safety Institute, Graz University of Technology, Inffeldgasse 13/6, 8010 Graz, Austria

<sup>b</sup> Department of Chemistry and Chemical Engineering, Chalmers University of Technology, Kemigården 4, 412 58 Gothenburg, Sweden

<sup>c</sup> Department of Bioproducts and Biosystems, Lignocellulose Chemistry, Aalto University, Puunjalostustekniikka 1, 00076 AALTO, Finland

### ARTICLE INFO

#### Keywords:

Meta-model  
Constitutive model  
Fibrous Network Structures  
Gradient Foams

### ABSTRACT

We introduce a novel *meta*-modelling approach coupled with a four-part piecewise constitutive model to predict the compressive behaviour of homogeneous foams using data from inhomogeneous specimens. This method estimates individual density layer responses within the foam, enabling the prediction of compression behaviour for ideal density configurations. Validated through cellulose pulp fibre foam experiments utilising Digital Image Correlation (DIC) analysis and finite element simulations of synthetic expanded polystyrene (EPS) foam, our *meta*-model effectively derives material properties from imperfect foams of varying densities, while accounting for errors induced by density variations. It accurately captures foam material response from initial compression through densification. Our approach offers significant advantages for optimising foam structures without costly commercial software or ideal specimens, bridging the gap between real-world materials and idealised models. While initially designed for cellulose pulp fibre foams, this model shows broad potential for evaluating various foams with density variations, including both sustainable and non-sustainable materials.

### 1. Introduction

Porous materials are commonly used and highly valued for their distinctive combination of low density, high specific strength and stiffness, making them ideal for lightweighting and energy absorption in automotive (Mkrtychyan et al., 2008) and aerospace applications (Li et al., 2000). Their high specific energy absorption capacity also makes them very valuable for impact attenuation in packaging (Nofar and Park, 2014) and personal safety equipment, such as helmets (Feist et al., 2024; de Sousa et al., 2012). The key mechanical property for most foam applications is therefore the compressive behaviour, both at low and high loading speeds.

Foams used in industrial applications are predominantly made from fossil-based materials, with metal foams also being widely utilised. Metal foams are particularly valued for high-energy impact absorption due to their superior initial stiffness and high plateau strength. However, increasing emphasis on sustainability has spurred research into bio-based and renewable alternatives. Cellulosic foams and pulp fibre network structures emerge as promising candidates, demonstrating potential in diverse applications (Chen et al., 2011; Ganesan et al., 2016).

Although many evaluations assume foams to be homogeneous and

isotropic, many, especially bio-based and metal foams, exhibit significant inhomogeneity (Kader et al., 2020). This is often due to variations in density distribution (Naeem et al., 2020; Palano et al., 2013; Wagner et al., 2025). These inhomogeneities can significantly impact the mechanical properties, and introduce orthotropic behaviour in the material. In some cases, intentional inhomogeneities, such as density gradients, are introduced to optimise foam performance for specific applications. Such gradient foams have been proposed for impact attenuation to reduce peak loads (Cui et al., 2009b; Cui et al., 2009a; Smeets et al., 2023; Zhu et al., 2023).

Commonly, these gradient foams are produced either by additive manufacturing (Xie et al., 2019) or through layered formulations with templates, including aqueous (Xu et al., 2024) or gelatine phases (Xie et al., 2019). However, a simpler approach to mimic such materials involves creating layered foam structures, with each layer having a distinct density. This approach is often employed in helmets (Forero Rueda et al., 2009) and metal foam stacks used in automotive crash-worthy structures (Salehi et al., 2022). Notably, natural porous materials like bamboo, palm wood, and bone exhibit similar density gradients, allowing them to retain high strength and stiffness, particularly under bending loads, while maintaining low overall densities

\* Corresponding author.

E-mail address: [florian.feist@tugraz.at](mailto:florian.feist@tugraz.at) (F. Feist).

<https://doi.org/10.1016/j.ijsolstr.2025.113522>

Received 12 December 2024; Received in revised form 13 April 2025; Accepted 10 June 2025

Available online 11 June 2025

0020-7683/© 2025 The Authors. Published by Elsevier Ltd. This is an open access article under the CC BY license (<http://creativecommons.org/licenses/by/4.0/>).

(Claussen et al., 2012; Wegst, 2011).

Cellulosic foams and pulp fibre network structures have been proposed as a sustainable material for impact absorbers, particularly in low-energy impact scenarios and packaging (Pääkkönen et al., 2024). These foams could replace a significant amount of fossil-based packaging materials, which are major contributors to environmental pollution and microplastic generation. However, severe difficulties to control the density have been observed in cellulose pulp fibre foams due to the production process. This often leads to an unintended gradient like foam configuration, which significantly influences their compressive behaviour (Wagner et al., 2025) and can lower the initial stiffness or reduce the energy absorption capacity below a desired level. Currently, it is challenging to determine whether the effort required to improve the production process is justified by the performance of the final product. Therefore, an early assessment of the potential of a porous material serves as a valuable tool.

Optimising gradient foams typically involves producing multiple foams with varying homogeneous densities, evaluating their compressive behaviour, fitting material laws to the observed responses, and subsequently interpolating the results (He et al., 2020).

While this approach is effective for generating optimised density distributions, it does require homogeneous specimens with various densities. This can be problematic when production-induced density distributions are difficult to control, which is the case with pulp fibre foams.

Constitutive material models which cover the properties of homogeneous foams over a wide density range have been explored in quasi-static (Duan et al., 2020) and dynamic settings (Liu et al., 2024), with some relying on machine learning (Frankel et al., 2022).

This work introduces a four-part piecewise constitutive model which aims to describe the compressive material behaviours of foam-like materials, without explicitly accounting for the underlying microstructure or material physics. This constitutive model is further employed within a novel *meta*-model approach to extract the stress–strain behaviour of density-constant foam based on experiments on density-variant foam samples. This approach enables the evaluation of ideally homogeneous foams using data from inhomogeneous and imperfect specimens. By predicting the material behaviour of a hypothetical homogeneous foam, it establishes a foundation for assessing the foam’s potential and allows for optimising foam stack properties without requiring high-quality specimens. Therefore, the need for an established process, which is capable of producing high quality, homogeneous specimens is diminished in the development of a novel porous material.

### 1.1. Background

Fibrous networks and foams share similarities in their macroscopic behaviour under compression, despite having distinct *meso*-mechanical structures. Fibrous networks consist of interconnected beam-like elements, while traditional foams are characterised by cell walls forming enclosed or partially enclosed voids. Polymer foam structures typically exhibit distinct deformation stages under compression: an initial elastic region, followed by a plateau region, and finally densification. In contrast, fibrous networks, particularly under out-of-plane loading, are monotonically increasing their stress with strain, showing no distinct plateau region.

In this work, we use the term “foam” broadly to encompass both traditional cellular foams with surface-like cell walls made from an isotropic base material, and fibrous network structures composed of interconnected (even anisotropic) beam-like elements and fibres. This generalisation allows us to apply similar modelling approaches to both types of porous structures, focusing on their macroscopic compressive behaviour rather than their specific micro-structural differences. This broader definition enables us to leverage existing foam mechanics theories while accounting for the unique characteristics of fibrous networks, particularly in the context of cellulose pulp fibre materials. By

doing so, we can develop a unified approach to modelling and predicting the compressive behaviour of various porous structures, regardless of their specific *meso*-scale morphology.

#### 1.1.1. Foam behaviour

Foam behaviour is typically characterised by three distinct regions: the initial stiffness region (I) (linear elastic in case of many polymeric cellular solids), the secondary stiffness region (II) (plateau region in case of polymeric cellular solids), and the tertiary region (III), often referred to as densification (Hwang et al., 2020; Kwon et al., 2021; Salimi Jazi et al., 2014) (Fig. 1a)). Various modelling approaches have been developed based on this classification (Alzoubi et al., 2014). The most widely used description comes from Gibson and Ashby. They provide equations for estimating the mechanical properties of foams based on their envelope density and the density of the base material (Gibson and Ashby, 2014).

These approximations allow for the prediction of the elastic modulus and plateau strength and provide a good approximation for open and closed cell polymer foams. The envelope elastic modulus of the foam ( $E^*$ ) can be estimated using the following equation:

$$\frac{E^*}{E_S} = C^* \left( \frac{\rho^*}{\rho_s} \right)^p \quad (1)$$

where  $E_S$  is the modulus of the solid material,  $C$  is a proportionality factor,  $\rho^*$  is the envelope foam density,  $\rho_s$  is the solid material density and  $p$  is the exponent ( $p \approx 2$ ).

These equations provide good approximations for both open and closed-cell foams. While they are most accurate for synthetic foams, they also enable reasonable predictions for a wide range of foam materials, such as nanofibrillar cellulose foams (Ali and Gibson, 2013). However, for pulp fibre foams the proportional factor  $C$  and exponent  $p$  can deviate significantly from values conventionally used for closed and open cell foams (Wagner et al., 2025). It is important to note that despite these deviations, the general power law relation still is quite accurate.

Gibson and Ashby further provide an equation (equation 2) for estimating the densification strain, which yields good predictions for a wide range of porous materials when compared to experimental results.

$$\epsilon_D \approx 1 - 1.4^* \frac{\rho^*}{\rho_s} \quad (2)$$

#### 1.1.2. Rule of Mixtures

The Rule of Mixtures (ROM) is a model used to estimate the elastic properties of composite materials that are reinforced with unidirectional continuous fibres. Based on Voigt’s isostrain assumption (Voigt, 1889), the longitudinal modulus ( $E_{11}$ ) of a composite can be expressed as:

$$E_{11} = E_f V_f + E_m V_m \quad (3)$$

where  $E_f$  and  $E_m$  represent the elastic moduli of the fibre and matrix respectively and  $V_f$  and

$V_m$  are their corresponding volume fractions.

To calculate the transverse elastic modulus ( $E_{22}$ ), Reuss’s isostress assumption (Reuss, 1929) is applied, which assumes that the transverse stress in both the fibres and matrix is equal. The transverse modulus ( $E_{22}$ ) is thus determined using the inverse Rule of Mixtures as follows:

$$E_{22} = \left( \frac{V_f}{E_f} + \frac{V_m}{E_m} \right)^{-1} \quad (4)$$

#### 1.1.3. Nelder-Mead optimisation technique

The Nelder-Mead optimisation technique (Nelder and Mead, 1965) is a widely used method for solving optimisation problems where the objective function is not easily differentiable. This method is especially advantageous for nonlinear optimisation problems that do not require derivatives of the objective function, making it ideal for functions that

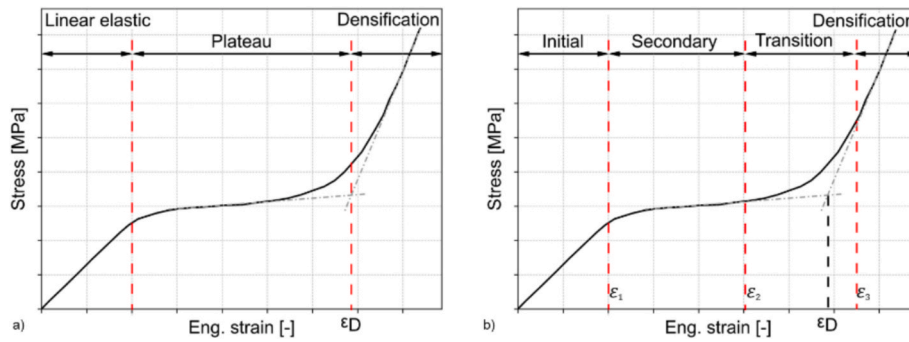


**Fig. 1.** a) Common polymer foam compressive stress–strain behaviour utilising three distinctive regions and b) proposed approach with four distinctive regions for foam-like materials in which the secondary region is described as linear however, does not necessitate a stress plateau.

are noisy, discontinuous, or not well-behaved in terms of gradient calculation. The Nelder-Mead algorithm proceeds iteratively, shrinking and adjusting the simplex, which represents a group of solutions, until convergence is achieved. Its applicability spans various domains, including engineering design optimisation, hyperparameter tuning in machine learning, and other scientific computations, where direct or gradient-based methods are impractical. However, it is important to note that this method may converge to local minima, especially in higher dimensional space. This limitation necessitates careful consideration when applying the method to high-dimensional optimisation problems.

## 2. Methods

### 2.1. Constitutive model

A four-part piecewise constitutive model was developed (illustrated in Fig. 1b)) to describe the compressive behaviour of foams. This model expands upon the traditional three regions commonly used for polymer foam materials (Hwang et al., 2020; Kwon et al., 2021; Salimi Jazi et al., 2014) by incorporating an additional transition region:

**Initial Stiffness Region:** The first region is assumed to be linear and only characterised by one stiffness value. The governing stiffness is representative of the Young’s modulus and the region encompasses the elastic region of a given foam.

**Secondary Stiffness Region:** The second region is also assumed to be linear, characterised by a stiffness value that is typically lower than the initial stiffness. While fibrous networks generally exhibit a monotonic increase in stress, polymeric foams often display a plateau in this region, with minimal stiffness. This phase is primarily responsible for energy absorption.

**Transition Region:** This region is non-linear and captures the onset of densification, modelled with a polynomial function. It is governed by the densification strain derived from the approximation provided by Gibson and Ashby and optimised using the coefficients of the transition region polynomial so that the overall function is close to continuous.

**Densification Region:** This is the final region where the foam is densified, leading to a steep increase in stress, which is also assumed to be linear.

The inclusion of the transition region allows for a more accurate description of the foam’s behaviour as it progresses from the secondary phase to the onset of densification, a characteristic that is particularly relevant for the evaluated bio-based foam material.

The mathematical definition of the four-piece piecewise function was described as follows:

$$\sigma_{(\epsilon)} = \begin{cases} \epsilon^* s_1, \epsilon < \epsilon_1 \\ (\epsilon - \epsilon_1)^* s_2 + \epsilon_1^* s_1, \epsilon < \epsilon_2 \\ a + b^* (\epsilon - \epsilon_2^* t_f) + d^* (\epsilon - \epsilon_2^* t_f)^{t_e}, \epsilon < \epsilon_3 \\ (\epsilon - \epsilon_3)^* s_3 + a + b^* (\epsilon - \epsilon_2^* t_f) + d^* (\epsilon - \epsilon_2^* t_f)^{t_e}, \epsilon \geq \epsilon_3 \end{cases} \quad (4)$$

In this equation,  $\sigma_{(\epsilon)}$  denotes the engineering stress as a function of strain. The parameters  $s_1$ ,  $s_2$ , and  $s_3$  represent the stiffness (or slope) of the initial (1), secondary (2), and densification (4) region respectively. The strain at which the linear elastic region transitions to the secondary region is denoted by  $\epsilon_1$ . The parameters  $\epsilon_2$  and  $\epsilon_3$ , which define the boundaries of the transition region, are calculated by utilising the estimated densification strain (equation 2) and a transition factor  $t_f$ .

$$\epsilon_2 = \epsilon_D - \epsilon_D^* t_f \quad (5)$$

$$\epsilon_3 = \epsilon_D + \epsilon_D^* t_f \quad (6)$$

The stress–strain relation of the transition region (3) is defined by the coefficients  $a$ ,  $b$ , and  $d$ , along with the transition exponent  $t_e$ , which governs the curvature of the transition region. These transition coefficients are computed to ensure continuity in the resulting function. This formulation enables a flexible representation of the foam’s mechanical behaviour as it moves from the secondary region to the densification phase. In total, six parameters are fitted for the constitutive model: three stiffness parameters, the boundary of the initial region, the transition factor, and the transition exponent. All other parameters, such as the densification strain, are either derived from previously established estimations or analytically calculated to maintain a continuous function. The four-part piecewise function was selected over alternatives, such as exponential functions, due to its superior ability to accurately capture the compressive behaviour of both polymer foam and fibrous networks. Although exponential functions can effectively capture the out-of-plane response of fibrous networks up to the onset of densification, which typically occurs at strains above 0.5 depending on the envelope density, they become less accurate beyond this point. Once densification is included, exponential functions, despite maintaining high overall accuracy, tend to inadequately represent the response in the pre-densification region (strains below approximately 0.5).

#### 2.1.1. Meta-modelling

The introduced meta-modelling approach proposes that inhomogeneous or gradient specimens with varying densities can be estimated as a layered foam stack of (nearly) homogeneous layers, as illustrated in Fig. 2. A constant density can therefore be assigned to each of the layers. A central assumption of this approach is the interchangeability of layers, which implies that the stacking sequence does not significantly influence the overall behaviour. This assumption is particularly valid under quasi-static, uniaxial compression, where the material stack does not exhibit substantial interfacial expansion mismatches between layers. Such mismatches could create complex multiaxial stress states, potentially

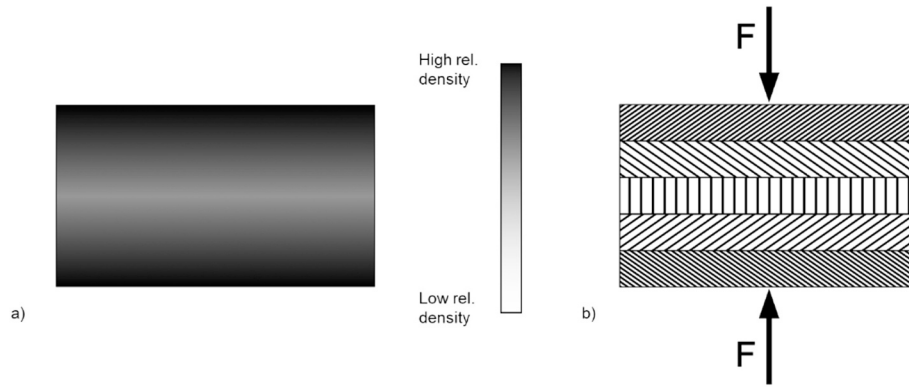


Fig. 2. a) Hypothetical density distribution in a foam specimen and b) corresponding layer-based model for applying Reuss's isostress assumption (Rule of Mixture for assessing transversal stiffness).

altering compressive behaviour. Three factors could theoretically invalidate this assumption by inducing multiaxial stress states: (1) High intrinsic Poisson's ratios within constituent layers, (2) sharp interfacial property contrasts, particularly in Poisson's ratios, and (3) severe stiffness gradients between adjacent layers. However, these conditions are unlikely in inhomogeneous foams, as they typically exhibit low Poisson's ratios and gradual variations in density and consequently in mechanical properties across layers. Furthermore, compressive stress–strain data from multiple specimens with differing envelope densities can be analysed simultaneously in order to derive better fitting coefficients for the material model.

This work builds upon and extends the seminal work of Gibson and Ashby (Gibson and Ashby, 2014) by implementing their density relationships within the *meta*-model framework. While Gibson and Ashby used a power law relationship to describe the initial stiffness, i.e. the Young's modulus of foams, we propose that the power law assumption also applies to the stiffness ( $s$ ) in the secondary and densification regions:

$$s_{nl} = c_n \cdot \left( \frac{\rho_l^*}{\rho_s} \right)^{p_n} \quad (7)$$

where the subscript  $n$  denotes the specific region of behaviour (i.e. 1 = initial, 2 = secondary and 3 = densification) and  $l$  denotes the layer (and therefore the density) for which the stiffness is calculated. This results in the computation of stiffness values for all layers at each region of behaviour. The stiffnesses are governed by the proportional factor  $c_n$  and the exponent  $p_n$  which are both defined for each region (but do not change across layers) and the ratio of the individual layer density  $\rho_l^*$  and the density of the base material, which is denoted by  $\rho_s$  and set to 1 500 kg/m<sup>3</sup> for cellulose and 1 000 kg/m<sup>3</sup> for polystyrene.  $E_s$  is included within the proportional factor  $c_n$  in contrast to equation 1.

A fundamental assumption of this model is that the power law exponent and proportional factor remain constant across varying densities, while potentially differing between the distinct stress–strain regions of the material.

By employing the Rule of Mixtures for a number of layers with known individual density and volume fraction, the model can extract detailed material parameters from the envelope foam stress–strain response. This approach enables a more comprehensive characterisation of the material's behaviour, accounting for density variations within the specimen. If it is assumed that the foam consists of only one layer, parameters are fitted which replicate the inhomogeneous foam behaviour for different envelope densities. However, in order to assess the properties of ideally homogeneous foams and therefore the actual foam material properties, it is necessary to introduce multiple layers, all of which utilising the four-part piecewise function in conjunction with the *meta*-model.

The response of each density layer within the specimen is fitted to the

constitutive model, allowing for the calculation of the resulting stress–strain curve. This is achieved by applying the Rule of Mixtures to the individual layers, specifically the out-of-plane (transversal) Rule of Mixtures is utilised. In this way, the methodology aggregates the contributions of individual layers with varying densities. Importantly, the accuracy of the evaluation is not inherently governed by the number of layers but rather by how accurately their number and densities are known. For stacked foams, the number of layers should, for optimal results, correspond to those found within the specimen. In contrast, for gradient foams, increasing the number of layers can improve accuracy, provided that the density distribution is known with sufficient precision.

This is shown in the following equation:

$$s^* = \left[ \frac{v_1}{s_1} + \frac{v_2}{s_2} + \dots + \frac{v_l}{s_l} \right]^{-1} \quad (8)$$

With  $s^*$  being the envelope stiffness,  $s_l$  being the stiffness and  $v_l$  being the volume fraction of each corresponding layer.

The model parameters are fitted to the experimental envelope stress–strain data from multiple imperfect foams or foam stacks using an in-house developed program. This program leverages the Nelder-Mead optimisation technique (Nelder and Mead, 1965) provided within the “Non-Linear Least-Squares Minimisation and Curve-Fitting for Python” library (LMFIT) (Newville et al., 2014). The software loads all available experimental envelope stress–strain responses of foam specimens along with their corresponding density distribution.

It simultaneously fits the *meta*-model parameters to maximise the coefficient of determination ( $R^2$ ) for the envelope behaviour (which is calculated from the individual layer responses) for all specimens, ensuring that the predicted envelope foam responses closely match the corresponding experimental data.

The fitting process only requires envelope stress–strain data and corresponding density distributions as inputs and is illustrated in Fig. 3 and the process proceeds as follows:

- Assumption of Coefficients:** The initial proportional factor  $c_n$  and the exponent  $p_n$  are generated using a random positive number for the initial, secondary and densification region.
- Calculating Coefficients in the Constitutive Model:** The *meta*-model coefficients are utilised to calculate the coefficients for the constitutive model (equation 4) for each layer within the data set (defined through the density input).
- Prediction of Layer Responses:** The equations within the constitutive model are solved, which generates a stress strain prediction for each layer within the provided density data.
- Computation of Envelope Response:** The envelope response of each specimen is calculated by combining the individual layer responses while utilising the volume fraction and following the Rule of Mixtures.

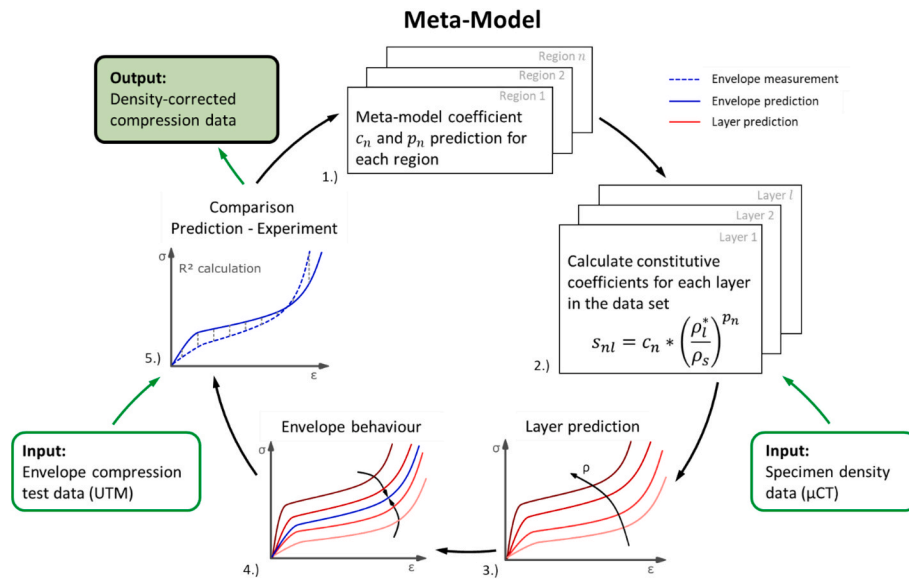


Fig. 3. Meta-model fitting process illustration.

5. **Comparison to Experimental Data:** The predicted specimen responses are compared to the experimentally observed envelope behaviour and an overall  $R^2$  value is computed. If the overall  $R^2$  value has reached a maximum, the fully parameterised model is returned.

1. **Updating of Coefficients:** If the optimum has not been reached, the coefficients of the *meta-model* are updated and the process continues.

Upon convergence to an optimal fit, the algorithm returns the optimised parameters, resulting in a fully defined model. This model accurately characterises the foam material's behaviour, accounting for density variations and encompassing a broad range of densities. The derived parameterisation facilitates precise prediction of stress-strain responses for diverse foam specimens.

To comprehensively assess the characteristics of the foam material while accounting for inherent inhomogeneities, multiple specimens, with significantly different envelope densities, were evaluated using the described *meta-model* approach.

## 2.2. Materials and foam characterisation

### 2.2.1. Density distribution

The primary material investigated in this study is a cellulose pulp fibre foam made from bleached softwood kraft pulp, which exhibits significant density inhomogeneities due to its production process. The foams were manufactured using the frothing method as described by Wagner et al. (Wagner et al., 2025).

Specimens with target envelope densities of 60, 80, 100, and 140 kg/m<sup>3</sup> were manufactured. Six cylindrical specimens with a diameter and height of 20 mm and envelope densities of 60, 80, and 140 kg/m<sup>3</sup> were placed into a 3D-printed PLA specimen holder and examined in terms of morphology with micro-computed tomography ( $\mu$ CT). The  $\mu$ CT analysis was performed using a UMITOM XL (Tescan) micro-computed tomography at a resolution of 15  $\mu$ m utilising a scan voltage of 40 kV and a current of 375  $\mu$ A. The  $\mu$ CT data was manually segmented to provide a detailed 3D distribution of the material within the foam volume. From this data, density variations have been derived for the 15  $\mu$ m high layers within the specimen. After assessing the densities of the individual scan layers for each specimen, the resulting distributions have been binned into nine groups and an average distribution has been calculated.

### 2.2.2. Compression testing and digital image correlation

Quasi-static out-of-plane compression tests were conducted to evaluate the compressive behaviour of the cellulose pulp fibre foams. For each of the four target envelope densities (60, 80, 100, and 140 kg/m<sup>3</sup>), four cube specimens with an edge length of 20 mm were prepared. The cubic geometry was chosen to facilitate 2D Digital Image Correlation (DIC) evaluation. Compression tests were performed using a ZPM-3000–500 Universal Testing Machine (UTM) from PCE Instruments, equipped with a TCTN-91110-3kN load cell. Each foam specimen was positioned between two flat compression plates for uniaxial compression testing. Tests were conducted under displacement-control at a constant loading velocity of 5 mm/min. at ambient conditions (21 °C and about 50 % RH). Fig. 4a) depicts the test setup.

2D DIC was utilised to capture the strain distribution for each foam specimen during compression (Fig. 4b)) in order to provide validation data. This data is only used in the validation and is not required for the proposed method. For this study, a DIC system equipped with a high-resolution (4 k, Lumix DMC-TZ101) camera was set up to monitor the deformation. To enable DIC tracking, a speckle pattern was applied to the surface of the foam specimens. This pattern was created by carefully spraying fine, water-based black paint droplets onto the specimens' surface. Care was taken to minimise water application, as cellulose fibres tend to disperse water based colour upon contact. Due to this dispersion the black paint resulted in a grey pattern on the white (bleached) fibres. The camera was positioned to capture the out-of-plane deformation, and the images were processed using the open-source DIC program "ICorrelation-2D Correlation" (de Deus Filho et al., 2022) (version v1.04.22). The parameters of the image acquisition and DIC properties are summarised in Table S1.

Prior to testing, the specimens were carefully inspected for surface imperfections of the cutting surface, to minimise loose fibre bundles, defined as fibres and fibre bundles attached only at one single point.

Furthermore, the Poisson's ratio over the deformation was analysed by comparing the in-plane strain results for each point with the corresponding out-of-plane strain, both of which were derived from the DIC analysis.

### 2.2.3. Model validation

The predicted envelope stress-strain curves were compared with the experimental envelope results, and the accuracy of the model was assessed using the root mean square error for these compression load curves. In addition to envelope foam behaviour, the model was used to

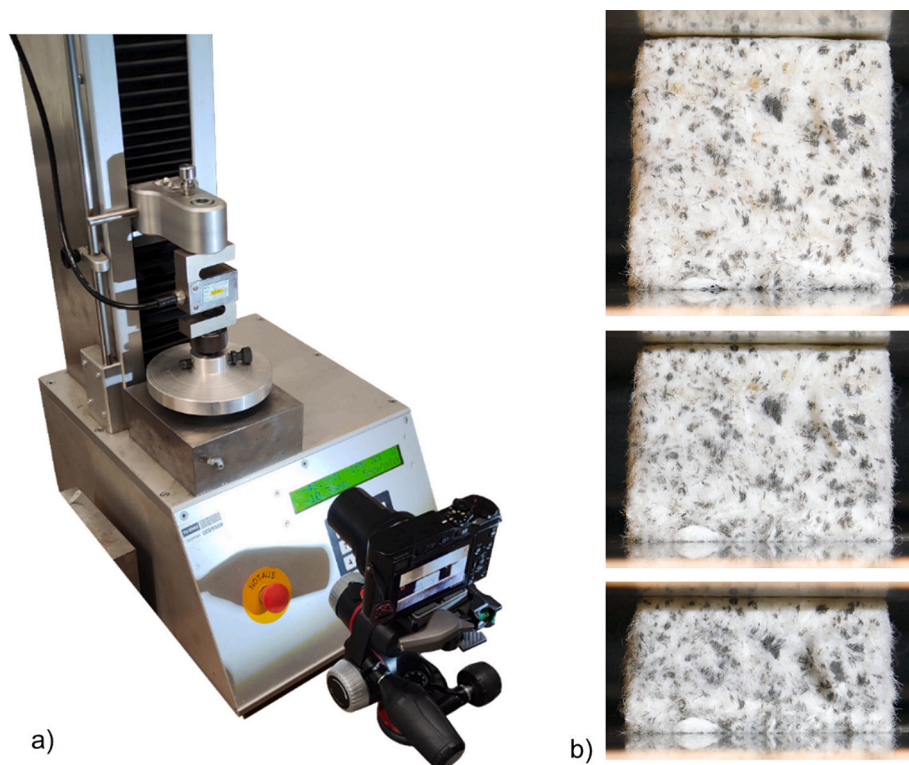


Fig. 4. a) Compression test setup and b) exemplary speckled foam specimen at various stages of deformation.

predict the stress–strain response of individual density layers within the foam. This layer-wise analysis was essential for assessing the behaviour of the overall homogeneous foam compressive behaviour. The predicted layer responses were compared with the DIC data to validate the model's accuracy. Additionally, the *meta*-model approach was tested on data generated from finite element method (FEM) simulations of expanded polystyrene (EPS) foam stacks. The simulations were performed with LS-Dyna (R13.1, smp, double precision) and the foam structures (20 x 20 x 20 mm<sup>3</sup> cubes with 15 layers in the height direction) consisted of elements with densities of 35, 50 and 70 kg/m<sup>3</sup> and were modelled utilising Mat83, which is a material model based on the unified constitutive laws proposed by Chang (Chang et al., 1998). Structures were generated with organized element distribution resulting in clearly defined, homogeneous, density layers and with randomly distributed element distribution in order to assess the impact of intra-layer variation on the model prediction. Simulations with ideal homogeneous foam cubes were simulated and used as a reference for evaluating the accuracy of the *meta*-model. Table 1 summarises the homogeneous and layer based simulation configurations, while Table S2 details the randomly distributed configuration.

This validation strategy provides a robust assessment of the *meta*-model's predictive capabilities and shows its potential applicability to a wide range of foam structures.

Table 1

Homogeneous and layer based simulation configurations.

| Nr.           | Envelope density [kg/m <sup>3</sup> ] | Volume fraction of 35, 50 and 70 kg/m <sup>3</sup> layers [%] |
|---------------|---------------------------------------|---|
| Reference 1   | 35                                    | 100, 0, 0   |
| Reference 2   | 50                                    | 0, 100, 0   |
| Reference 3   | 70                                    | 0, 0, 100   |
| Layer stack 1 | 52                                    | 33, 33, 33  |
| Layer stack 2 | 42                                    | 73, 13, 13  |
| Layer stack 3 | 51                                    | 13, 73, 13  |
| Layer stack 4 | 63                                    | 13, 13, 73  |

### 3. Results and Discussion

#### 3.1. Density distribution

The 3D datasets from the micro-CT (shown in Fig. 5a)) were evaluated and the resulting layer-based volume distribution for each specimen were utilised to calculate a relative density distribution. The scans showed a general reduction in x-ray absorption values near the edges of the scan volume. This artefact in the absorption (greyscale) data was most likely introduced by the PLA specimen holder, which bordered the outer diameter regions of the scan volume. To address this issue, manual segmentation was performed rather than utilising the greyscale values directly. This approach differs from the method used by Afshar et al. (2023), who reported that lower scan resolutions are sufficiently accurate for density distribution analysis when derived from absorption values (Afshar et al., 2023). However, the segmentation based method produced very similar results in the out-of-plane density distribution analysis to a comparison based on absorption values, as shown in Fig. S1, while accounting for the influence of the specimen holder and was therefore utilised.

To assess density variation, equal-frequency binning was applied to the relative density distribution. This method constructs bins such that each bin contains an equal number of data points. These results are shown in Fig. 5b). This approach effectively emulates the discrete layer averaging inherent in DIC evaluations, facilitating comparability.

It is important to note an average density distribution has been used. While individual density distributions for each specimen could potentially offer higher accuracy, an averaged density distribution was deemed preferable for the evaluated pulp fibre foams. This choice is partly motivated by the observed variance in density distribution among foam samples with identical envelope densities. The use of an averaged distribution of the six evaluated specimens also considers practical constraints: CT scans are expensive, limiting the number of specimens that can be analysed in detail and CT scans preferentially require cylindrical specimens. Furthermore, mechanical testing was conducted on

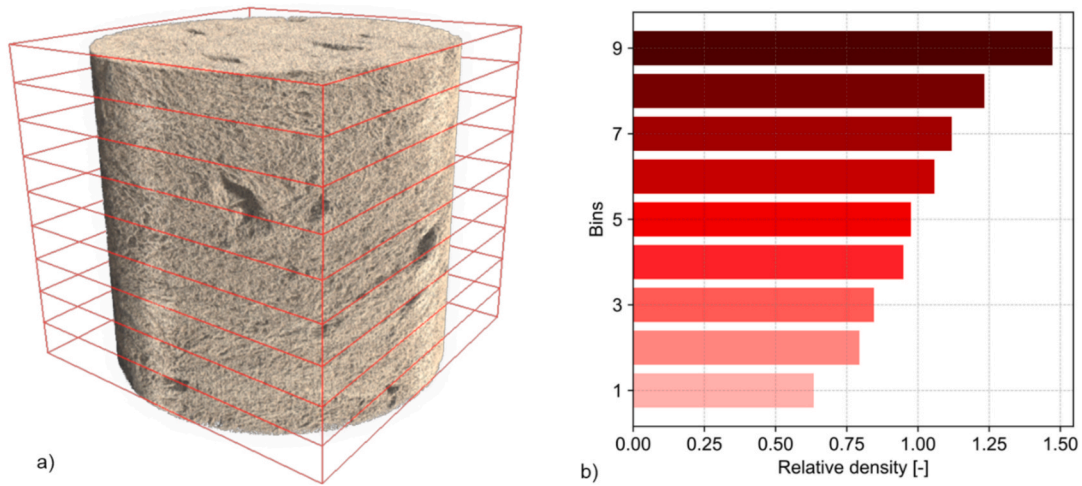


Fig. 5. a) Segmentation in individual density layers b) normalised density distribution of the layers.

cubic specimens, as the two-dimensional DIC setup requires a planar surface for accurate evaluation and therefore cannot be used to directly generate validation data from the cylindrical CT specimens. Consequently, averaging the density distributions was necessary since no compressive validation data was available for those particular specimens.

### 3.2. DIC analysis

DIC was performed with a mesh size (Fig. 6a) similar to the chosen layer height of the density distribution assessment. The strain analysis has shown strong inhomogeneities over the specimen surface and deformation patterns, which indicate a layered compression response (Fig. 6b) and d)).

Analysis of the DIC results for each layer reveals a distinct stress–strain response, as illustrated in Fig. 7. A staggered compression behaviour was observed among all specimens, reflecting the density distribution and its influence on the local compliance of the structure.

The DIC analysis indicated that the evaluated pulp fibre foams exhibit a Poisson’s ratio under 0.04 for engineering strains below 0.4. This indicated that shear phenomena due to transverse strain have very limited effect in the first half of compression. The use of a commercial-grade 4 K colour camera (Lumix DMC-TZ101) for the DIC evaluation presents a limitation, as such cameras generally exhibit higher inaccuracies compared to professional monochromatic CCD cameras. These inaccuracies are primarily due to the demosaicing process inherent to colour cameras, which involves interpolation and introduces increased noise in the recorded light intensity data, which is used in the correlation process (Forsey and Gungor, 2016). Additional errors may arise from the use of a rolling shutter, where pixels are not read out simultaneously.

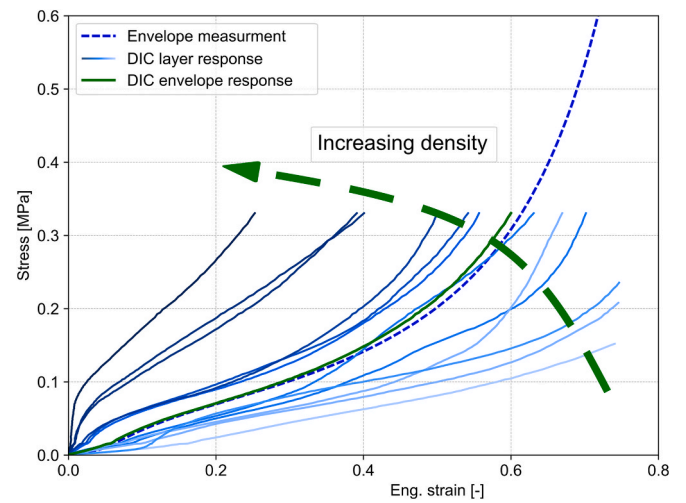


Fig. 7. Example of measured DIC results for each layer (shades of blue), ranging from low-density layers (light-coloured) to high-density layers (dark-coloured), shown alongside the corresponding stress–strain curve from the UTM (blue dashed line) and the calculated mean DIC response (green).

However, numerous studies have shown that modern high-resolution cameras can still achieve sufficient accuracy (Arza-García et al., 2022; Gödek and Tosun Felekoğlu, 2023; Hedayati et al., 2017; Kosmann et al., 2019; Li et al., 2020), especially when employed for slow deformations and large strain evaluations (Pritchard et al., 2013), as is the case in this work.

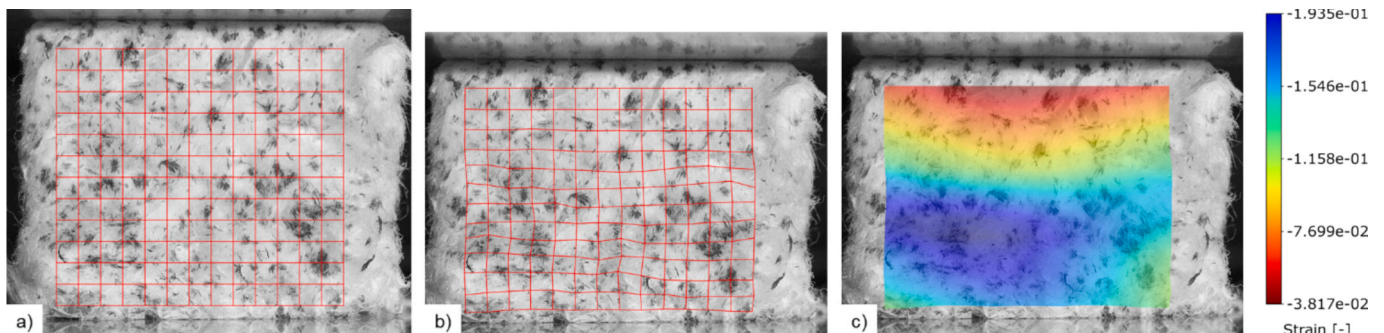


Fig. 6. a) DIC mesh in the uncompressed state and b) at 0.12 compressive engineering strain. c) Strain distribution at 0.12 compressive engineering strain.

One additional drawback of this method is the assumption that the surface displacement is representative of the whole volume. While edge effects may be minimal, especially in the case of synthetic foams, the evaluated fibre foam may exhibit loose fibres or fibre bundles. Such fibres may move in a transverse direction without undergoing deformation. Consequently, they should be removed prior to testing, which may result in minor damage to the material. Therefore, experiments where these loose fibres were present have been excluded. Another limitation of the chosen evaluation is the limited accuracy particularly at high strains. This is caused by the incremental correlation scheme, which was utilised in the DIC analysis. While this method enables the tracking of large deformations, it is susceptible to compounding errors since these errors can accumulate over successive evaluation steps rather than being referenced to an initial frame (Zhou et al., 2014). Consequently, we limited the DIC evaluation shown Fig. 7 to engineering strains below 0.75 to avoid excessive errors associated with incremental DIC analysis.

### 3.3. Constitutive model and meta-model predictions

The behaviour of the foams exhibiting significant density variations can be accurately replicated utilising the introduced four-part piecewise equation. When fitting the experimental data directly to the proposed constitutive model, a very good correlation is observed, with the lowest  $R^2$  value of the twelve samples being 0.964, which occurs only for high density ( $140 \text{ kg/m}^3$ ) specimens (Fig. 8b)). Specimens with densities of  $100 \text{ kg/m}^3$  and lower reach a  $R^2$  value of at least 0.997 (e.g.  $60 \text{ kg/m}^3$  with an  $R^2$  value of 0.998 shown in Fig. 8a)). The minor reduction of the correlation with increased density could possibly be attributed to increased transverse strain effects at higher densities.

The high  $R^2$  values show that the function is well-suited for capturing the overall envelope behaviour of the foam. Notably, the newly introduced transition region was essential for this success; omitting this transition phase renders the approach unsuitable, as evidenced by  $R^2$  values falling below 0.5.

The main benefit of this approach arises when utilising the *meta*-model to derive the individual layer-wise stress-strain responses. Fig. 9 illustrates the results from the *meta*-model for a specimen with a density of  $60 \text{ kg/m}^3$  (Fig. 9a) and  $140 \text{ kg/m}^3$  (Fig. 9b)). The reaction of the layer-wise analysis are plotted in red lines, with darker shades representing higher density layers. It is noteworthy that low density layer reactions in the  $60 \text{ kg/m}^3$  foam show almost identical stiffnesses in the initial and secondary region, while higher density layers exhibit more pronounced degenerative behaviour over those two regions. In other words: The higher density foams exhibited pronounced strain softening (see detail view in the respective plots).

Table 2 summarises the evaluated parameters of the *meta*-model

(equations 4–7) for both the layer-wise evaluation (predicted ideal homogeneous behaviour) and the envelope-wise evaluation. In the latter, the same model parameters are assessed without accounting for density variations within the sample, essentially extracting the model parameters directly from the experimental results. It is apparent that the model coefficients differ significantly when comparing the two evaluations. It is important to note that, although the transition region plays a crucial role in the overall processes, it is the least sensitive to changes in evaluation methodology.

It is crucial to emphasise that compression tests of foams and porous structures with significant density variations across their thickness, yielding an average density of  $x$ , cannot be directly used to predict the behaviour of a quasi-homogeneous foam with negligible density variation and the same average density  $x$ . In other words, the apparent behaviour, or homogenised behaviour, differs substantially from the true behaviour of a homogeneous-density foam. This discrepancy is particularly evident in the primary stiffness, which can be strongly influenced by the compliance of less dense layers. The strength of the presented tool lies in its ability to predict the “true” behaviour of assumed density-invariant porous structures, even when the test specimens themselves exhibit density variance. This capability allows for more accurate modelling and understanding of material properties, independent of manufacturing-induced density variations. This benefit is also shown in Table 3, which reports the estimated moduli of the initial region for the apparent foam behaviour and the homogeneous foam prediction.

The findings underscore that density variations across a foam’s thickness can lead to behaviours that differ significantly from those of a uniform foam with the same average density.

An additional benefit of the outlined method is that it is returning data for a broader density range than the evaluated envelope densities. While the assessment of inhomogeneous foams covers only the range between the lowest and highest envelope density (in our case  $60$  to  $140 \text{ kg/m}^3$ ), the layer-based approach extends the range from  $40$  to  $190 \text{ kg/m}^3$ .

Material responses for ideally homogeneous densities can be derived by applying the fitted coefficients shown in Table 3 to equation 7, in order to derive the density-dependent stiffness values ( $s_1, s_2$  and  $s_3$ ) for each region. These density dependent stiffnesses can subsequently be utilised in the four-part piecewise constitutive model in conjunction with the other fitted coefficients (i.e.  $t_e$  and  $t_f$ ) while the transition coefficients  $a$ ,  $b$ , and  $d$  can either be extracted from the returned fitting results or once again analytically solved in such a fashion that a continuous, differentiable, function is derived.

These results are shown in the surface plots in Fig. 10 which allows for assessing material performance under ideal conditions and

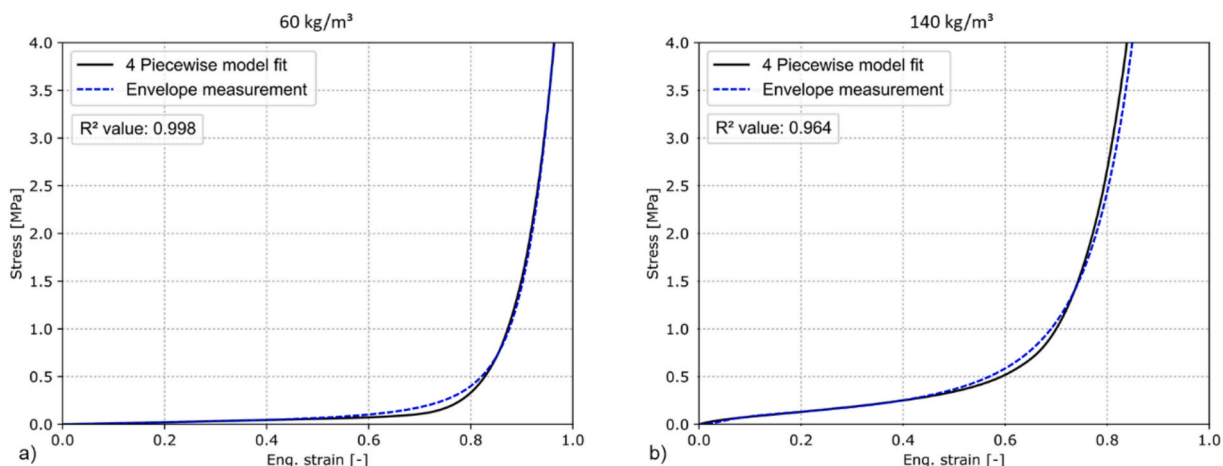


Fig. 8. Piecewise function directly fitted to experimental results for a) a  $60 \text{ kg/m}^3$  dense specimen and a b)  $140 \text{ kg/m}^3$  dense specimen.

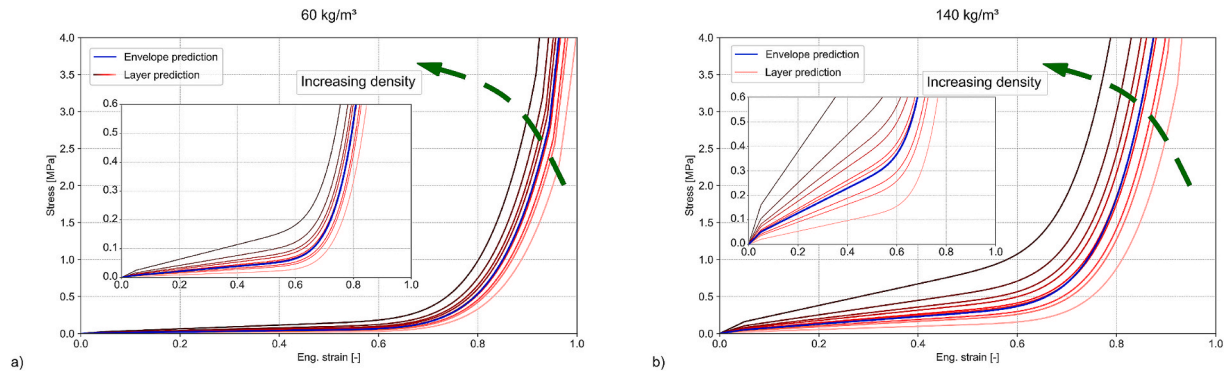


Fig. 9. Predictions for the compressive behaviour (blue) of foams with envelope densities of (a) 60 kg/m<sup>3</sup> and (b) 140 kg/m<sup>3</sup>, derived from the estimation of individual layer responses (shades of red), ranging from low-density layers (light-coloured) to high-density layers (dark-coloured).

Table 2

Comparison between layer-wise assessment yielding homogeneous foam parameters and the envelope-wise, inhomogeneous evaluation.  $c$  denoting the proportional coefficient and  $p$  the exponent of equation 7, for regions 1 through 3.  $t_f$  denoting the transition factor of equation 5 and 6 and  $t_e$  the transition exponent in equation 4.

| Meta parameter | Layer-wise assessment | Envelope-wise assessment | Difference |
|----------------|-----------------------|--------------------------|------------|
| $c_1$ [MPa]:   | 456.55                | 264.27                   | 73 %       |
| $p_1$ [-]:     | 2.41                  | 2.374                    | 1 %        |
| $c_2$ [MPa]:   | 150.97                | 115.93                   | 30 %       |
| $p_2$ [-]:     | 2.25                  | 2.15                     | 5 %        |
| $t_e$ [-]:     | 5.82                  | 5.26                     | 11 %       |
| $t_f$ [-]:     | 0.42                  | 0.46                     | -9 %       |
| $c_3$ [MPa]:   | 148.57                | 104.65                   | 42 %       |
| $p_3$ [-]:     | 0.50                  | 0.40                     | 26 %       |

Table 3

Change in initial modulus determined for ideally homogeneous foams using a layer-wise assessment, and for inhomogeneous specimen using an envelope-wise assessment.

| Example density [kg/m <sup>3</sup> ] | Layer-wise modulus [MPa] | Envelope-wise modulus [MPa] | Difference |
|--------------------------------------|--------------------------|-----------------------------|------------|
| 40                                   | 0.074                    | 0.048                       | 53 %       |
| 60                                   | 0.197                    | 0.127                       | 55 %       |
| 80                                   | 0.393                    | 0.251                       | 57 %       |
| 100                                  | 0.673                    | 0.426                       | 58 %       |

evaluating whether the material is suitable for a given application as a homogeneous foam. By utilising the fitted parameters and changing the density distribution in the program, foam stack optimisation can be performed.

However, it is important to note that the discretisation of the individual layers still represents some degree of averaging. The accuracy of this approach depends on the density distribution used in the model, which may have inherent spread or variation.

### 3.4. Validation

To demonstrate that the layer-wise estimation provides a reasonable approximation, the estimated responses are overlaid with the results from the DIC. Although slight deviations from the assumed distribution are expected due to potential variations in DIC layer densities, Fig. 11 shows that the general behaviour is well captured. Deviations in densification behaviour can most likely be attributed to the limited accuracy of the DIC evaluation in high-strain regions. Small deviations in the overall behaviour are also logical, due to using an averaged density distribution rather than one for each specimen.

As an additional validation, envelope stress-strain data from the EPS foam stack simulations with different envelope densities and varying volume fractions (Table 1, layer stack 1 through 4, illustrated in Fig. 12b) through e)) have been analysed. The evaluated envelope-wise stress-strain curves, along with the corresponding envelope- and layer-wise densities and volume fractions of the foam stacks, were used as

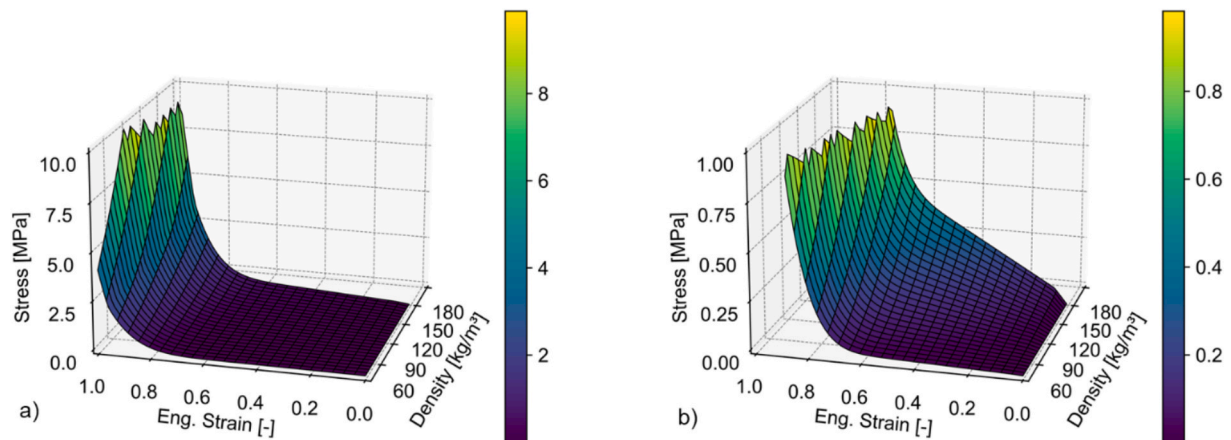
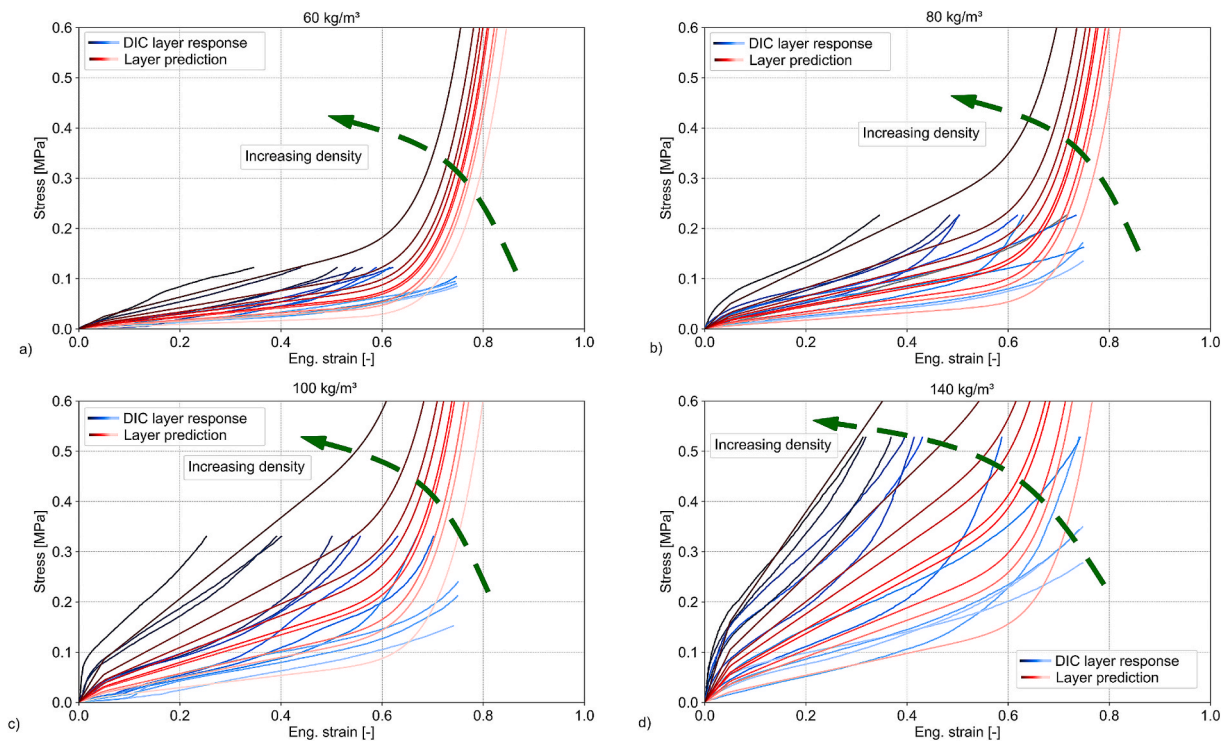


Fig. 10. Surface plot of the assessed foam material behaviour a) from initial to densification and b) as a detailed view for the initial and secondary region.



**Fig. 11.** Fitting results (shades of red) for each density layer are shown, with light-colored lines representing low-density layers and dark-colored lines representing high-density layers. These are overlaid with corresponding results from the DIC evaluation (shades of blue) for foams with envelope densities of (a) 60, (b) 80, (c) 100, and (d) 140  $\text{kg/m}^3$ .

input data for the fitting algorithm. The approximated layer-wise behaviour correlated well with the foam behaviour from the reference simulations (Table 1, reference 1 through 3) which is shown in Fig. 12a). This demonstrates that the *meta*-model predictions are of very high quality, provided that sufficiently accurate density distributions are known.

The layer interchangeability was also examined through simulations, which confirmed that altering the layer sequence does not affect the overall mechanical response when using the EPS material model. It is important to note that the material model proposed by Chang, which was employed, assumes a Poisson's ratio of zero. Additional simulations were conducted using an alternative material model that allows for non-zero Poisson's ratios. As anticipated, when the Poisson's ratio was zero, the results were invariant with respect to the foam layer stack sequence. A parameter study showed that for higher Poisson's ratios (up to 0.4) and significant stiffness differences between layers, where high-density foam is twice as stiff as low-density foam, small variations in compressive stress (around 2 %) may occur. However, under different loading conditions, such as dynamic loading or non-uniaxial compression, the layer sequence may have a more pronounced effect. Dynamic phenomena like viscoelasticity and inertia, as well as variations in load distribution (e.g., when using cylindrical or spherical impactors), could lead to deviations in material behaviour depending on the layer configuration. Further, the effect of intra-layer density distribution was evaluated by analysing the results from the randomly distributed simulations (Fig. 13 b) and c)). For the three randomly distributed configurations, the corresponding density of each layer was provided as an input file for the *meta*-model. Fig. 13a) illustrates the results of the 15 individual layer responses from the simulation, shown as the grey-shaded area, and overlays it with the red-shaded area representing the predicted responses. It can be observed that, although the general

behaviour is well captured, significantly larger deviations occur due to the intra-layer density distribution. Nevertheless, the results still provide a reasonable approximation of the behaviour of individual foam layers.

#### 4. Conclusion

A novel *meta*-modelling approach has been developed and validated to predict the nearly density-constant, layer-wise compressive behaviour of cellulose pulp fibre foams from compression tests on foams with significant density variations. This *meta*-model employs a four-part piecewise constitutive model, accurately capturing the compressive behaviour of foams across a wide range of densities and strains.

This newly developed *meta*-model accurately captures the response from initial compression through densification and enables predictions of the behaviour of individual, nearly homogeneous density layers.

This offers a useful approximation of the potential of porous, foam-like materials, where controlling the density distribution during production is often challenging. The method provides data which can be leveraged for optimising foam structures and assessing their suitability for potential applications. A key advantage of this approach is that it does not rely on high-quality foam samples or expensive commercial software.

Although the model is specifically tailored to bulky cellulose-based network structures, it shows potential for broader application, particularly for synthetic foams with inhomogeneities and gradient foams. This work deepens our understanding of how density variations influence foam behaviour and presents new opportunities for the development of sustainable, high-performance materials across diverse industrial applications.

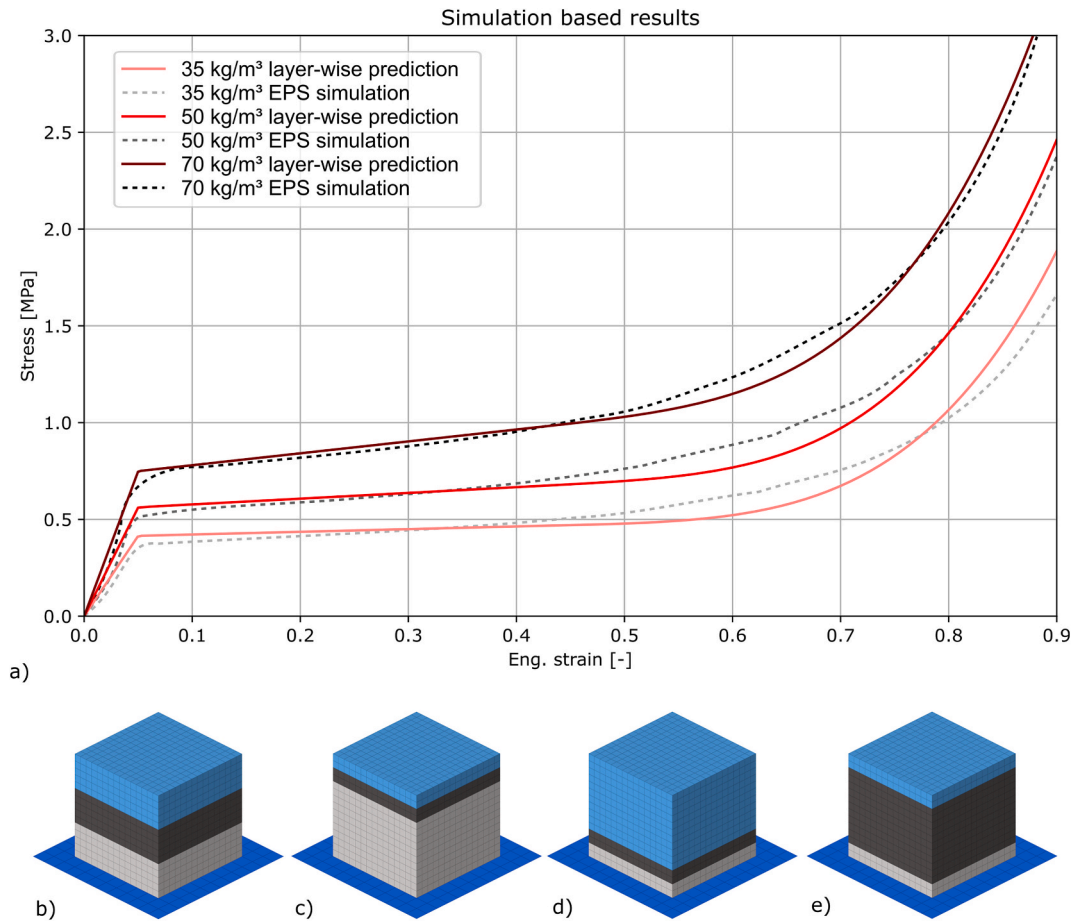


Fig. 12. a) Predicted ideal homogeneous material compressive stress–strain curves comparison with results from ideal EPS simulations for densities of 35, 50 and 70 kg/m<sup>3</sup>. Illustration of simulation configurations from which the stress–strain curves have been used as an input for the *meta*-model: b) Layer stack 1, c) Layer stack 2, d) Layer stack 3, e) Layer stack 4. White elements represent 35 kg/m<sup>3</sup>, blue elements represent 50 kg/m<sup>3</sup> and black elements represent 70 kg/m<sup>3</sup>.

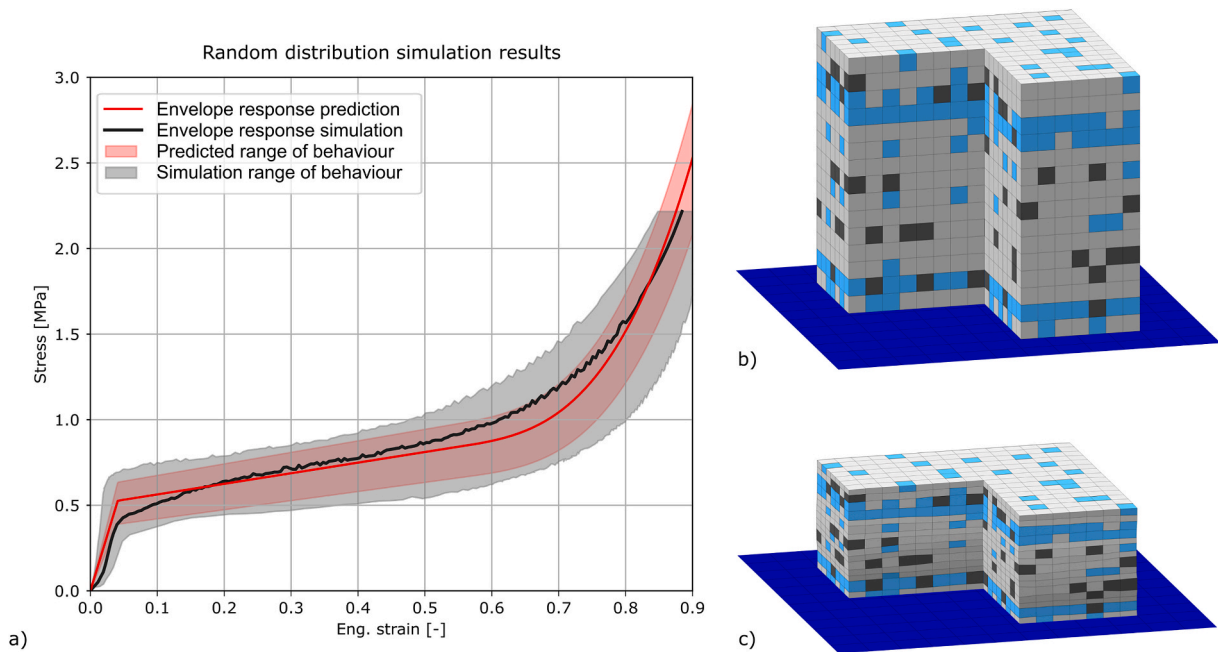


Fig. 13. a) Comparison of the simulation results (grey) and *meta*-model predictions (red) for 15 individual foam layers. Example of a randomly distributed EPS foam cube b) in uncompressed state and c) compressed, where white elements represent 35 kg/m<sup>3</sup>, blue elements represent 50 kg/m<sup>3</sup> and black elements represent 70 kg/m<sup>3</sup>.

## CRediT authorship contribution statement

**Markus Wagner:** Writing – original draft, Visualization, Software, Methodology, Investigation, Formal analysis, Data curation. **Sebastian Wurm:** Writing – review & editing, Investigation. **Georg Baumann:** Writing – review & editing, Conceptualization. **Tiina Nypelö:** Writing – review & editing, Funding acquisition. **Florian Feist:** Writing – review & editing, Supervision, Project administration, Conceptualization.

## Declaration of competing interest

The authors declare that they have no known competing financial interests or personal relationships that could have appeared to influence the work reported in this paper.

## Acknowledgement

This work has received funding from the European Union's Horizon 2020 research and innovation programme under grant agreement No 964430.

## Appendix A. Supplementary data

Supplementary data to this article can be found online at <https://doi.org/10.1016/j.ijisolstr.2025.113522>.

## Data availability

Data will be made available on request.

## References

- Afshar, R., Stjärnesund, J., Gamstedt, E.K., Giralanda, O., Sahlén, F., Tjahjanto, D., 2023. A micro-CT investigation of densification in pressboard due to compression. *Strain* 59, e12442. <https://doi.org/10.1111/str.12442>.
- Ali, Z.M., Gibson, L.J., 2013. The structure and mechanics of nanofibrillar cellulose foams. *Soft Matter* 9, 1580–1588. <https://doi.org/10.1039/C2SM27197D>.
- Alzoubi, M.F., Al-Hallaj, S., Abu-Ayyad, M., 2014. Modeling of compression curves of flexible polyurethane foam with variable density, chemical formulations and strain rates. *J. Solid Mech.* 6, 82–97.
- Arza-García, M., Núñez-Temes, C., Lorenzana, J.A., Ortiz-Sanz, J., Castro, A., Portela-Barral, M., Gil-Docampo, M., Bastos, G., 2022. Evaluation of a low-cost approach to 2-D digital image correlation vs. a commercial stereo-DIC system in Brazilian testing of soil specimens. *Archiv.Civ.Mech.Eng* 22. <https://doi.org/10.1007/s43452-021-00325-0>.
- Chang, F.S., Song, Y., Lu, D.X., DeSilva, C.N., 1998. Unified constitutive equations of foam materials. *J. Eng. Mater. Technol.* 120, 212–217. <https://doi.org/10.1115/1.2812345>.
- Chen, W., Yu, H., Li, Q., Liu, Y., Li, J., 2011. Ultralight and highly flexible aerogels with long cellulose I nanofibers. *Soft Matter* 7, 10360. <https://doi.org/10.1039/c1sm06179h>.
- Claussen, K.U., Scheibel, T., Schmidt, H.-W., Giesa, R., 2012. Polymer gradient materials: can nature teach us new tricks? *Macro Materials & Eng* 297, 938–957. <https://doi.org/10.1002/mame.201200032>.
- Cui, L., Forero Rueda, M.A., Gilchrist, M.D., 2009a. Optimisation of energy absorbing liner for equestrian helmets. Part II: functionally graded foam liner. *Mater. Des.* 30, 3414–3419. <https://doi.org/10.1016/j.matdes.2009.03.044>.
- Cui, L., Kiernan, S., Gilchrist, M.D., 2009b. Designing the energy absorption capacity of functionally graded foam materials. *Mater. Sci. Eng. A* 507, 215–225. <https://doi.org/10.1016/j.msea.2008.12.011>.
- de Deus Filho, J.C.A., Da Silva Nunes, L.C., Xavier, J.M.C., 2022. iCorrVision-2D: an integrated python-based open-source digital image Correlation software for in-plane measurements (Part 1). *SoftwareX* 19, 101131. <https://doi.org/10.1016/j.softx.2022.101131>.
- Duan, Y., Zhao, X., Du, B., Shi, X., Zhao, H., Hou, B., Li, Y., 2020. Quasi-static compressive behavior and constitutive model of graded foams. *Int. J. Mech. Sci.* 177, 105603. <https://doi.org/10.1016/j.ijmeosci.2020.105603>.
- Feist, F., Wagner, M., Baumann, G., Spirk, S., Biegler, V., Jiang, Q., Nypelö, T., 2024. A cellulosic fibre foam as a bicycle helmet impact liner for brain injury mitigation in oblique impacts. *Heliyon*, e40790. <https://doi.org/10.1016/j.heliyon.2024.e40790>.
- Forero Rueda, M.A., Cui, L., Gilchrist, M.D., 2009. Optimisation of energy absorbing liner for equestrian helmets. Part I: layered foam liner. *Mater. Des.* 30, 3405–3413. <https://doi.org/10.1016/j.matdes.2009.03.037>.
- Frankel, A., Hamel, C.M., Bolintineanu, D., Long, K., Kramer, S., 2022. Machine learning constitutive models of elastomeric foams. *Comput. Methods Appl. Mech. Eng.* 391, 114492. <https://doi.org/10.1016/j.cma.2021.114492>.
- Ganesan, K., Dennstedt, A., Barowski, A., Ratke, L., 2016. Design of aerogels, cryogels and xerogels of cellulose with hierarchical porous structures. *Mater. Des.* 92, 345–355. <https://doi.org/10.1016/j.matdes.2015.12.041>.
- Gibson, L.J., Ashby, M.F. (Eds.), 2014. *Cellular Solids*. Cambridge University Press.
- Gödek, E., Tosun Felekoglu, K., 2023. Effect of Camera Resolution on the Determination of Mechanical and Multiple Crack Properties of Engineered Cementitious Composites via Digital Image Correlation. *Hittite Journal of Science and Engineering* 10, 117–124. <https://doi.org/10.17350/HJSE19030000298>.
- He, S., Lv, Y., Chen, S., Dai, G., Liu, J., Huo, M., 2020. Gradient regulation and compressive properties of density-graded aluminum foam. *Mater. Sci. Eng. A* 772, 138658. <https://doi.org/10.1016/j.msea.2019.138658>.
- Hedayati, N., Madoliat, R., Hashemi, R., 2017. Strain measurement and determining coefficient of plastic anisotropy using digital image correlation (DIC). *Mechanics & Industry* 18, 311. <https://doi.org/10.1051/meca/2016060>.
- Hwang, B.-K., Kim, S.-K., Kim, J.-H., Kim, J.-D., Lee, J.-M., 2020. Dynamic compressive behavior of rigid polyurethane foam with various densities under different temperatures. *Int. J. Mech. Sci.* 180, 105657. <https://doi.org/10.1016/j.ijmeosci.2020.105657>.
- Kader, M.A., Hazell, P.J., Brown, A.D., Tahtali, M., Ahmed, S., Escobedo, J.P., Saadatfar, M., 2020. Novel design of closed-cell foam structures for property enhancement. *Addit. Manuf.* 31, 100976. <https://doi.org/10.1016/j.addma.2019.100976>.
- Kosmann, J., Völkerink, O., Schollerer, M.J., Holzhiuter, D., Hühne, C., 2019. Digital image correlation strain measurement of thick adherend shear test specimen joined with an epoxy film adhesive. *International Journal of Adhesion and Adhesives* 90, 32–37. <https://doi.org/10.1016/j.ijadhadh.2019.01.024>.
- Kwon, S.-B., Kim, J.-D., Lee, J.-M., 2021. A void growth- and coalescence-dependent anisotropic damage model for polymeric foams. *Continuum Mech. Thermodyn.* 33, 545–561. <https://doi.org/10.1007/s00161-020-00926-9>.
- Li, C., Luo, H., Pan, B., 2020. High-throughput measurement of coefficient of thermal expansion using a high-resolution digital single-lens reflex camera and digital image correlation. *The Review of scientific instruments* 91, 105106. <https://doi.org/10.1063/5.0013496>.
- Li, Q.M., Mines, R., Birch, R.S., 2000. The crush behaviour of rohacell-51WF structural foam. *Int. J. Solids Struct.* 37, 6321–6341. [https://doi.org/10.1016/S0020-7683\(99\)00277-2](https://doi.org/10.1016/S0020-7683(99)00277-2).
- Liu, X., Wang, Y., He, X., Liu, H., Cao, S., 2024. Deformation failure mechanism and constitutive model of gradient aluminum foam under impact loading. *Compos. Struct.* 327, 117684. <https://doi.org/10.1016/j.compstruct.2023.117684>.
- Mkrtchyan, L., Maier, M., Huber, U., 2008. Structural polyurethane foam: testing and modelling for automotive applications. *Int. J. Crashworthiness* 13, 523–532. <https://doi.org/10.1080/13588260802221310>.
- Naeem, M.A., Gábor, A., Mankovits, T., 2020. Influence of the manufacturing parameters on the compressive properties of closed cell aluminum foams. *Period. Polytech., Mech. Eng.* 64, 172–178. <https://doi.org/10.3311/PPme.16195>.
- Nelder, J.A., Mead, R., 1965. A simplex method for function minimization. *Comput. J.* 7, 308–313. <https://doi.org/10.1093/comjnl/7.4.308>.
- Newville, M., Stensitzki, T., Allen, D.B., Ingarigola, A., 2014. LMFIT: Non-Linear Least-Square Minimization and Curve-Fitting for Python. <https://doi.org/10.5281/zenodo.11813>.
- Nofar, M., Park, C.B., 2014. Poly (lactic acid) foaming. *Prog. Polym. Sci.* 39, 1721–1741. <https://doi.org/10.1016/j.progpolymsci.2014.04.001>.
- Pääkkönen, E., Ketoja, J.A., Paltakari, J., 2024. Energy absorption and resilience in quasi-static loading of foam-formed cellulose fibre materials. *Cellul.* 31, 7137–7152. <https://doi.org/10.1007/s10570-024-06030-4>.
- Palano, F., Nobile, R., Dattoma, V., Panella, F.W., 2013. Fatigue behaviour of aluminium foam sandwiches. *Fatigue Fract. Eng. Mat. Struct.* 36, 1274–1287. <https://doi.org/10.1111/ffe.12063>.
- Pritchard, R.H., Lava, P., Debruyne, D., Terentjev, E.M., 2013. Precise determination of the Poisson ratio in soft materials with 2D digital image correlation. *Soft matter* 9, 6037. <https://doi.org/10.1039/c3sm50901j>.
- Reuss, A., 1929. Berechnung der fließgrenze von mischkristallen auf grund der plastizitätsbedingung für einkristalle. *Zeitschrift Für Angewandte Mathematik Und Mechanik* 9, 49–58. <https://doi.org/10.1002/zamm.19290090104>.
- Salehi, M., Mirbagheri, S.M.H., Jafari Ramiani, A., 2022. Experimental, theoretical, and Numerical investigations into the compressive behavior of multi-layer metallic foam filled tubes. *J. Mater. Eng. Perform* 31, 3723–3740. <https://doi.org/10.1007/s11665-021-06475-9>.
- Salimi Jazi, M., Rezaei, A., Karami, G., Azarmi, F., Ziejewski, M., 2014. A computational study of influence of helmet padding materials on the human brain under ballistic impacts. *Comput. Methods Biomech. Biomed. Eng.* 17, 1368–1382. <https://doi.org/10.1080/10255842.2012.748755>.
- Smeets, M., Kauvaka, P., Uddin, K., Koohbor, B., Youssef, G., 2023. Full-Field analyses of density-graded Elastomeric foams under quasistatic and impact loadings. *Adv. Eng. Mater.* 25, 2300994. <https://doi.org/10.1002/adem.202300994>.
- de Sousa, R.A., Gonçalves, D., Coelho, R., Teixeira-Dias, F., 2012. Assessing the effectiveness of a natural cellular material used as safety padding material in motorcycle helmets. *Simulation* 88, 580–591. <https://doi.org/10.1177/0037549711414735>.
- Voigt, W., 1889. Ueber die beziehung zwischen den beiden elasticitätsconstanten isotroper körper. *Annalen der Physik* 274, 573–587. <https://doi.org/10.1002/andp.18892741206>.
- Wagner, M., Biegler, V., Wurm, S., Baumann, G., Nypelö, T., Bismarck, A., Feist, F., 2025. Pulp fibre foams: morphology and mechanical performance. *Compos. A Appl. Sci. Manuf.* 108515. <https://doi.org/10.1016/j.compositesa.2024.108515>.

- Wegst, U.G.K., 2011. Bending efficiency through property gradients in bamboo, palm, and wood-based composites. *J. Mech. Behav. Biomed. Mater.* 4, 744–755. <https://doi.org/10.1016/j.jmbbm.2011.02.013>.
- Xie, C., Gao, Q., Wang, P., Shao, L., Yuan, H., Fu, J., Chen, W., He, Y., 2019a. Structure-induced cell growth by 3D printing of heterogeneous scaffolds with ultrafine fibers. *Mater. Des.* 181, 108092. <https://doi.org/10.1016/j.matdes.2019.108092>.
- Xu, Y., Tang, L.e., Nok-langthong, C., Wagner, M., Baumann, G., Feist, F., Bismarck, A., Jiang, Q., 2024. Functionally gradient macroporous polymers: emulsion templating offers control over density, pore morphology, and composition. *ACS Appl. Polym. Mater.* 6, 5150–5162. <https://doi.org/10.1021/acsapm.4c00261>.
- Zhou, Y., Sun, C., Chen, J., 2014. Adaptive subset offset for systematic error reduction in incremental digital image correlation. *Opt. Lasers Eng.* 55, 5–11. <https://doi.org/10.1016/j.optlaseng.2013.10.014>.
- Zhu, L., Wang, G., Xu, Z., Li, X., Yang, C., Zhao, G., 2023. A new microcellular foaming strategy to develop structure-gradient thermoplastic polyurethane foams with enhanced elasticity. *Mater. Des.* 234, 112325. <https://doi.org/10.1016/j.matdes.2023.112325>.